ACS Macro Letters

pubs.acs.org/macroletters Letter

Charge-Transfer-Induced Self-Assembly of Doped Conjugated Block Copolymer Nanofibers

Karnati Narasimha,[§] Shine K. Albert,[§] Jongwook Kim, Hyojung Kang, Sungsu Kang, Jungwon Park, JaeHong Park, and So-Jung Park*

Cite This: *ACS Macro Lett.* 2023, 12, 382−388 Read Online

ACCESS | Metrics & More | Article Recommendations | Supporting Information

ABSTRACT: Here, we report charge-transfer-driven self-assembly of conjugated block copolymers (BCP) into highly doped conjugated polymer nanofibers. The ground-state integer charge transfer (ICT) between a BCP composed of poly(3-hexylthiophene) and poly(ethylene oxide) (P3HT-*b*-PEO) and electron-deficient 2,3,5,6-tetrafluoro-7,7,8,8-tetracyanoquinodimethane (F4TCNQ) induced spontaneous self-assembly of the donor and the acceptor into well-defined one-dimensional nanofibers. The presence of the PEO block plays an important role for the self-assembly by providing a polar environment that can stabilize nanoscale charge transfer (CT) assemblies. The doped nanofibers were responsive to various external stimuli such as heat, chemical, and light and exhibited efficient photothermal properties in the near-IR region. The CT-driven BCP self-assembly reported here provides a new platform for the fabrication of highly doped semiconductor nanostructures.

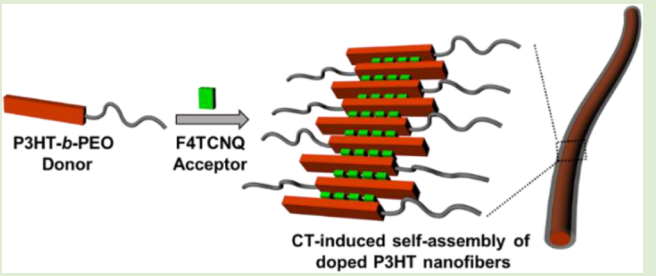

Molecular doping is gaining increasing attention as a promising avenue for controlling optoelectronic properties of conjugated polymers.[1−6] In this approach, small molecule dopants oxidize or reduce host polymers, creating integer charge-transfer (ICT) sites. Ground state charge transfer (CT) gives rise to new or improved functionalities for a number of applications such as field-effect transistors,[7] photovoltaics,[8] ferroelectrics,[9,10] thermoelectric devices,[11−15] and photopatterning.[16,17] An important challenge in this field is the difficulty in controlling the molecular packing and nanoscale morphology of doped organic semiconductors, which exert a significant impact on their functionalities. Currently, molecular doping is typically performed by depositing polymers and dopants from an organic solution. However, it is difficult to control the doping level and molecular packing structure using the conventional codeposition process, because the polymer−dopant ion pair tends to aggregate into disordered structures with abundant and persistent defects.[18]

Here, we report the fabrication of one-dimensional (1D) assemblies of highly doped conjugated polymers by ICT-induced cocrystallization of a molecular dopant, 2,3,5,6-tetrafluoro-7,7,8,8-tetracyanoquinodimethane (F4TCNQ), and a conjugated block copolymer (BCP) composed of poly(3-hexylthiophene) and poly(ethylene oxide) (P3HT-*b*-PEO) (Scheme 1).[18−20] Self-assembly of conjugated BCP has emerged as a promising route for the formation of well-defined nanostructures of conjugated polymers.[21−26] For example, we and others have previously shown that well-defined 1D nanofibers can be formed from the solution-phase self-

Scheme 1. Schematic Showing the Charge-Transfer-Driven Self-Assembly of the Donor (D) Poly(3-hexylthiophene)-*block*-poly(ethylene oxide) (P3HT-*b*-PEO) and the Acceptor (A) 2,3,5,6-Tetrafluoro-7,7,8,8-tetracyanoquinodimethane (F4TCNQ)

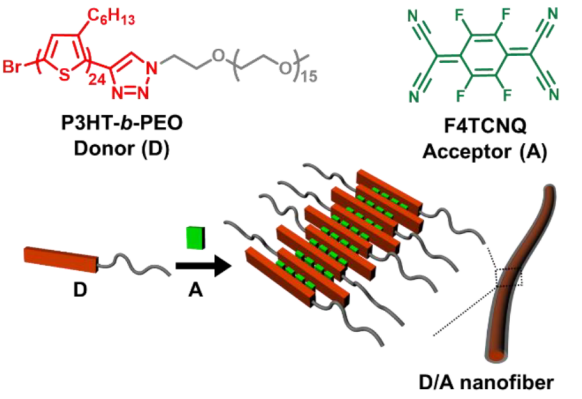

Received: December 20, 2022
Accepted: February 26, 2023

https://doi.org/10.1021/acsmacrolett.2c00752
ACS Macro Lett. 2023, 12, 382−388

assembly of P3HT BCPs.[21,27,28] More complex structures, such as segmented nanofibers showing long-range exciton transport, have been fabricated by the seeded crystallization of two different conjugated BCPs.[29,30] Reversible self-assembly of conjugated BCP nanofibers was realized by incorporating functional polymers responsive to external stimuli such as light or redox agents.[23,31,32] Herein, we report that the block copolymer architecture of P3HT-*b*-PEO promotes the CT interaction between the P3HT donor (D) and the F4TCNQ acceptor (A), leading to the formation of well-defined donor/acceptor (D/A) nanofibers. This new approach provides a promising pathway to the fabrication of highly doped organic semiconductor nanostructures having useful properties for a number of electronic,[5,7,8] optoelectronic,[6] and photothermal[9] applications.

P3HT-*b*-PEO was synthesized by a click reaction following our previously published method.[21] Briefly, ethynyl-terminated regioregular P3HT was synthesized by the Grignard metathesis (GRIM) polymerization method[33] and coupled with azide-terminated poly(ethylene oxide) (PEO, number-average molecular weight (M_n): 750 g/mol) by a copper-catalyzed click reaction to yield P3HT-*b*-PEO (Scheme S1).[21] Synthesized monomers and polymers were characterized by nuclear magnetic resonance (NMR; Figures S1-S4) and gel permeation chromatography (GPC). The M_n of P3HT was determined by GPC to be 4000 (dispersity ($Đ$): 1.19; Figure S9a), yielding $P3HT_{24}$-*b*-PEO_{16}. For comparison, another BCP composed of P3HT and polydimethylsiloxane ($P3HT_{26}$-*b*-$PDMS_{11}$) was synthesized by coupling azide-terminated polydimethylsiloxane (PDMS, M_n: 1000 g/mol) and ethynyl-terminated P3HT (M_n: 4300 g/mol, $Đ$: 1.23, Figure S9b). More synthetic details and characterization data are provided in the Supporting Information (Figures S5–S8).

F4TCNQ was chosen as the acceptor because its LUMO (−5.24 eV) is slightly lower than the HOMO of P3HT (∼−5 eV), which allows an efficient ground-state CT to form a F4TCNQ radical anion ($F4TCNQ^{\bullet-}$) and a P3HT positive polaron ($P3HT^{\bullet+}$).[34] In a typical procedure, self-assembly of P3HT-*b*-PEO and F4TCNQ was induced by simply mixing P3HT-*b*-PEO and F4TCNQ in toluene at a weight ratio of 1:1. Upon mixing, the color of the solution turned dark brown, suggesting the formation of D/A CT complexes (Figure 1a). The UV–vis absorption spectra of the P3HT-*b*-PEO/F4TCNQ mixture showed the characteristic absorption band of nonaggregated single-chain P3HT at 450 nm and that of F4TCNQ at 387 nm (Figure 1b). In addition to the signature bands of P3HT and F4TCNQ, the P3HT-*b*-PEO/F4TCNQ mixture exhibited a sharp double-peak feature at 775 and 850 nm over a broad band covering 700–900 nm (Figure 1b), which were assigned to the F4TCNQ radical anion ($F4TCNQ^{\bullet-}$) and the P3HT hole polaron ($P3HT^{\bullet+}$), respectively. The spectroscopic fingerprints in the near-infrared (NIR) region indicate a ground state ICT between P3HT and F4TCNQ. Complete quenching of P3HT photoluminescence at 570 nm with the addition of F4TCNQ also supports efficient CT interactions (Figure 1c).[35,36] The ground state CT was also confirmed by X-band electron paramagnetic resonance (EPR) spectroscopy (Figure 1d). The P3HT-*b*-PEO/F4TCNQ mixture showed an EPR signal with a *g*-factor of 2.001 from P3HT radical cations,[28,18] which was absent in the P3HT-*b*-PEO spectrum without F4TCNQ. The EPR data serves as clear evidence for the existence of polarons generated by the ground state ICT between P3HT and F4TCNQ. In addition, the near-infrared (NIR) and Fourier transform-infrared (FT-IR) spectra of the P3HT-*b*-PEO/F4TCNQ mixture showed broad bands in the NIR region, indicating the presence of hole polarons (Figure S10). The spectral features also support the stacked D/A structure proposed in Scheme 1.[20,37–40]

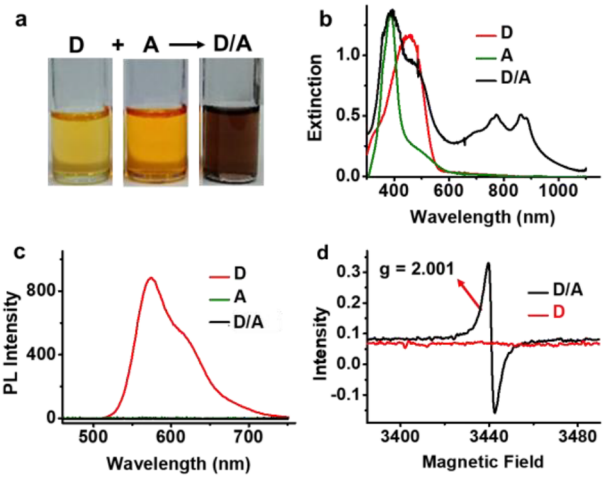

Figure 1. Self-assembly of the P3HT-*b*-PEO donor (D) and the F4TCNQ acceptor (A) in toluene (0.05 mg/mL, 1:1 D:A weight ratio). (a) Photographic images. (b) UV–vis absorption spectra. (c) Photoluminescence emission spectra (λ_{ex}: 440 nm). (d) EPR spectra of D/A and D in toluene (0.2 mg/mL, 1:1 D:A weight ratio).

A number of spectroscopic measurements was carried out to optimize the self-assembly conditions. First, the $P3HT^{\bullet+}$/$F4TCNQ^{\bullet-}$ bands increased with time and saturated after ∼6 h for a typical D/A concentration of 0.05 mg/mL (Figure 2a). Accordingly, the incubation time for the D/A mixture was set

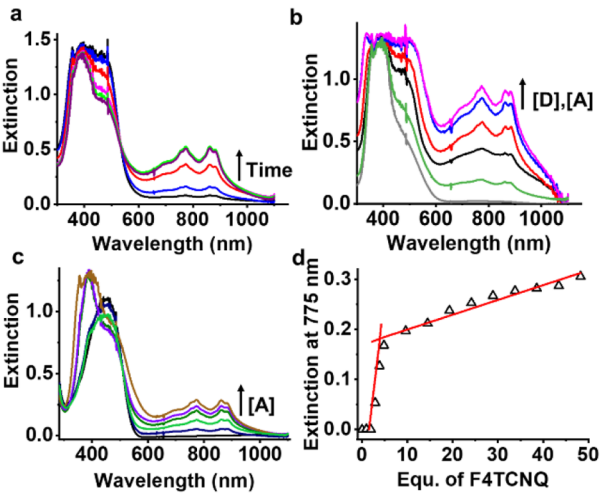

Figure 2. CT complexes formed at varying conditions. (a) UV–vis spectra of D/A mixtures (0.05 mg/mL) taken over time (black: 0.1 h, blue: 0.5 h, red: 1 h, magenta: 6 h, green: 12 h, purple: 24 h). (b) UV–vis spectra of D/A mixtures formed at different concentrations (in mg/mL in toluene) of D and A (gray: 0.01, green: 0.02, black: 0.04, red: 0.06, blue: 0.08, magenta: 0.1). (c) UV–vis spectra of D/A mixtures at varying concentrations of A with a constant [D] = 0.04 mg/mL (concentration of F4TCNQ: 0, 0.01, 0.0125, 0.0375, 0.05, 0.125 mg/mL). (d) Absorbance changes in (c) at 775 nm plotted against the number of moles of F4TCNQ per 1 mol of P3HT-*b*-PEO.

https://doi.org/10.1021/acsmacrolett.2c00752
ACS Macro Lett. 2023, 12, 382–388

to 12 h. Second, the P3HT$^{\bullet+}$/F4TCNQ$^{\bullet-}$ bands increased with the concentrations of P3HT-*b*-PEO and F4TCNQ, and they began to appear at a fairly low concentration ($\lesssim$0.02 mg/mL, Figure 2b). Note that both P3HT-*b*-PEO and F4TCNQ are well-dissolved in toluene at low concentration, and therefore, self-assembly at such conditions ensures the formation of pure CT assemblies. Third, the maximum doping level was determined from concentration-dependent UV−vis spectroscopy measurements carried out for a series of F4TCNQ concentrations (0.002−0.1 mg/mL) at a constant P3HT-*b*-PEO concentration of 0.04 mg/mL (Figure 2c). The P3HT$^{\bullet+}$/F4TCNQ$^{\bullet-}$ bands steeply increased with the amount of F4TCNQ until the D:A molar ratio reached 1:4 (Figures 2d and S11), followed by a gradual increase. This result indicated that about four F4TCNQ molecules were incorporated per one P3HT-*b*-PEO, which is reasonable considering that the degree of polymerization of P3HT used in this study was 24 and hole polarons are known to span over about four monomer units in P3HT.[41]

We anticipated that the ground state ICT between P3HT and F4TCNQ might mediate the organization of P3HT-*b*-PEO and F4TCNQ, generating well-defined nanoscale assemblies. Figure 3a presents the transmission electron microscopy (TEM) image of D/A assemblies formed by dissolving 0.05 mg of P3HT-*b*-PEO and F4TCNQ in 1 mL of toluene and aging the solution for 24 h at room temperature, which show 1D nanofiber structures. Scheme 1 describes the molecular packing structure of the D/A assemblies based on the spectroscopic and TEM data, which is composed of alternating P3HT and F4TCNQ units shielded with a PEO shell. The average width of nanofibers was 15 ± 2 nm on TEM (Figures 3a and S12), which was somewhat larger than the length of $P3HT_{24}$ (9.6 nm) calculated with a monomer length of 0.4 nm.[21,42] In previous studies of P3HT-*b*-PEO nanofibers formed by the addition of a nonsolvent, the fiber width matched fairly well with the length of P3HT.[21] The slight difference in the calculated and observed widths observed here was attributed to the misalignment of P3HT caused by the insertion of F4TCNQ. The 1D assembly structure was maintained at high concentrations of D and A (Figures 3b and S13), which was further confirmed by AFM measurements (Figures 3c and S13d). When the amount of F4TCNQ relative to that of P3HT-*b*-PEO was increased to a D:A weight ratio of 1:2, nanofibers with a rough surface were observed (Figure S14), presumably due to the deposition of excess F4TCNQ on D/A nanofibers.

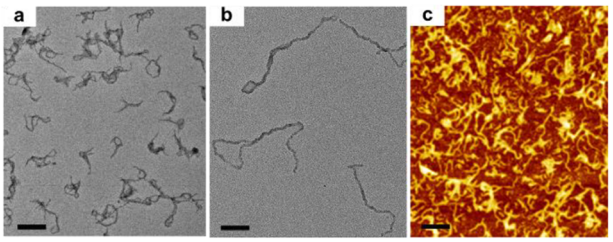

Figure 3. Nanofibers formed from CT-induced assembly of P3HT-*b*-PEO and F4TCNQ. (a, b) TEM image of CT nanofibers formed at D/A concentration 0.05 mg/mL (scale bar: 200 nm) (a) and 0.2 mg/mL (b). (c) AFM image of CT fibers at a D/A concentration 0.2 mg/mL (scale bar: 1 μm).

It is important to note that the ICT-induced self-assembly occurred in a condition where both P3HT-*b*-PEO and F4TCNQ remain well-solubilized without aggregation when they are separately dissolved in toluene. Therefore, the assembly procedure used in this study ensures the formation of pure CT assemblies. As mentioned above, self-assembly of P3HT-*b*-PEO can be induced by adding a nonsolvent for P3HT, such as water or acetonitrile (ACN), which generates nanofibers composed of a P3HT core and a PEO shell.[21] The polymer-only assemblies exhibit red-shifted absorption bands due to the increased planarity with clear vibronic structures resulting from the $\pi-\pi$ stacking between P3HT (Figure S15).[21] Such spectroscopic signatures of P3HT aggregates are absent in the D/A assemblies studied here (Figure 1b). These spectroscopic data confirm that the nanofibers in P3HT-*b*-PEO/F4TCNQ mixture are purely D/A assemblies and are consistent with the assembly formed through the stacking of F4TCNQ between P3HT, as described in Scheme 1. These results contrast with previously reported F4TCNQ-doped P3HT nanofibers formed by introducing F4TCNQ to preformed nanofibers of P3HT homopolymers.[17,19,27,43] It was found that CT complex formation between soluble P3HT and F4TCNQ is a slow process, and preaggregation of P3HT is required for efficient doping of F4TCNQ presumably due to the delocalization of hole polarons in P3HT aggregates. In the previous studies,[17,43] P3HT nanofibers maintain the molecular packing structure after doping, which is supported by the vibronic peaks of P3HT aggregates, and F4TCNQ dopants were assumed to bind at the periphery of P3HT nanofibers.

To investigate the role of the block copolymer architecture in promoting ICT interactions, control experiments were conducted with P3HT homopolymers (M_n: 4000 g/mol; $Đ$: 1.19) and P3HT-*b*-PDMS, a BCP with a relatively nonpolar block. Figure 4a presents the UV−vis spectra of a P3HT/F4TCNQ mixture (0.05 mg/mL in toluene) along with those of P3HT and F4TCNQ at the same concentration. Interestingly, the P3HT/F4TCNQ mixture did not show the P3HT$^{\bullet+}$/F4TCNQ$^{\bullet-}$ bands observed in the P3HT-*b*-PEO/F4TCNQ. Rather, the absorption spectra were simply the combination of the spectra of P3HT and F4TCNQ. This result is consistent with previous reports showing that P3HT$^{\bullet+}$/F4TCNQ$^{\bullet-}$ complex formation is slow in solution.[43] Similarly, the extinction spectra of P3HT-*b*-PDMS/F4TCNQ lacked any noticeable F4TCNQ$^{\bullet-}$/P3HT$^{\bullet+}$ bands (Figure 4b). The corresponding emission spectra showed a decrease in emission intensity of P3HT (Figure 4c,d). However, the degree of quenching was substantially lower than that observed for P3HT-*b*-PEO showing complete quenching (Figure 1c). As the concentration of P3HT/F4TCNQ was increased above 0.06 mg/mL, weak absorption bands corresponding to F4TCNQ$^{\bullet-}$ and P3HT$^{\bullet+}$ started appearing in the extinction spectra (Figure 4e). However, their intensities were significantly smaller than those of P3HT-*b*-PEO at the same concentration. Similar trends were observed for P3HT-*b*-PDMS (Figure 4f). In addition, P3HT homopolymers and P3HT-*b*-PDMS formed irregular aggregates rather than well-defined nanofibers (Figure S16). These results indicate that the PEO block effectively promotes CT interactions between P3HT and F4TCNQ and reinforces the formation of well-defined 1D assembly structures. We attributed this behavior to the amphiphilic nature of the PEO block.[1] First, the PEO shell promotes self-assembly of P3HT-*b*-PEO and F4TCNQ by providing a polar environment that can stabilize P3HT$^{\bullet+}$/

https://doi.org/10.1021/acsmacrolett.2c00752
ACS Macro Lett. 2023, 12, 382−388

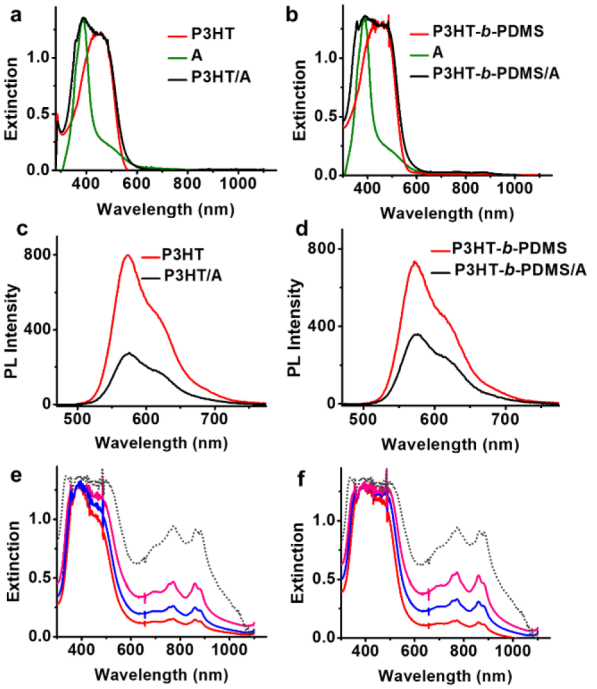

Figure 4. Self-assembly of P3HT (a, c, e) or P3HT-*b*-PDMS (b, d, f) with F4TCNQ acceptor (A). (a) Extinction spectra of P3HT, A, and P3HT/A (0.05 mg/mL). (b) Extinction spectra of P3HT-*b*-PDMS, A, and P3HT-*b*-PDMS/A (0.05 mg/mL). (c) Emission spectra of P3HT and P3HT/A (0.05 mg/mL). (d) Emission spectra of P3HT-*b*-PDMS and P3HT-*b*-PDMS/A (0.05 mg/mL). (e, f) Extinction spectra of P3HT/A (e) and P3HT-*b*-PDMS/A (f) at different concentrations (red: 0.06, blue: 0.08, pink: 0.1 mg/mL, weight ratio 1:1). Extinction spectra of P3HT-*b*-PEO/A formed at 0.1 mg/mL are given for comparison (gray dotted line).

$F4TCNQ^{\bullet-}$ ion pairs (Scheme 1). Second, PEO is a unique polymer soluble in a broad range of solvents from water to toluene. While P3HT and F4TCNQ are soluble in toluene, $P3HT^{\bullet+}/F4TCNQ^{\bullet-}$ ion pairs are insoluble in nonpolar solvents and thus they tend to precipitate out of toluene. For P3HT-*b*-PEO, the PEO shell can shield $P3HT^{\bullet+}/F4TCNQ^{\bullet-}$ ion pairs, preventing them from macroscopic aggregation.

While the D/A assemblies were stable over months at ambient conditions (Figure S17), the assembly was reversibly controllable by applying external stimuli. The temperature-dependent UV−vis spectra of D/A nanofibers showed a gradual reduction in intensity of the $P3HT^{\bullet+}/F4TCNQ^{\bullet-}$ bands with temperature up until ∼40 °C, at which point the $P3HT^{\bullet+}/F4TCNQ^{\bullet-}$ bands steeply decreased, reaching almost zero intensity at 80 °C (Figure S18a,c), consistent with the literature data on F4TCNQ-doped P3HT films.[16] The ICT band regained its intensity with the temperature decrease, showing the thermal reversibility of D/A assemblies (Figure S18b). Additionally, the chemical responsivity was examined by reacting D/A assemblies with a strong electron donor, KI, which resulted in the formation of green precipitates. The spectral data of the supernatant confirmed the dissociation of D/A assemblies as the loss of spectral signatures corresponding to $F4TCNQ^{\bullet-}/P3HT^{\bullet+}$ in the UV−vis spectrum and the rise of the characteristic emission peak of P3HT to 98% in the PL spectra (Figure S19). Such responsive properties can be useful for patterning applications.[16,17]

The PL quenching of D/A nanofibers indicates dissipation of the excited state energy through nonradiative relaxation channels, which can result in an efficient photothermal effect.[16,44−47] To test the hypothesis, D/A fibers prepared by mixing 0.05 mg/mL of P3HT-*b*-PEO and F4TCNQ in toluene were subjected to irradiation at two different laser wavelengths, 532 and 808 nm, corresponding to the P3HT and $P3HT^{\bullet+}/F4TCNQ^{\bullet-}$ absorption bands, respectively (Figure 5). The

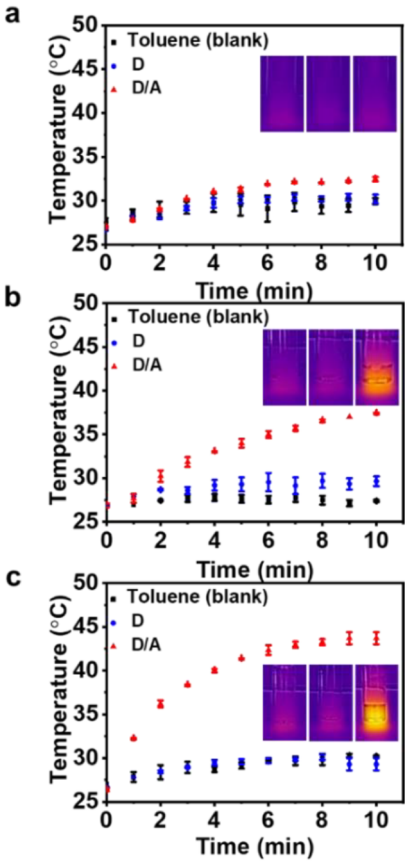

Figure 5. Photothermal effect of the D/A assemblies. (a, b) Photothermal data of D/A fibers formed at 0.05 mg/mL in toluene when irradiated with 532 nm (a) and 808 nm (b) laser. (c) Photothermal data of D/A fibers formed at 0.2 mg/mL in toluene when irradiated with an 808 nm laser. The data for control samples of P3HT-*b*-PEO (D) and toluene (blank) are provided for comparison.

same measurements were carried out for control samples of P3HT-*b*-PEO (D) and toluene as well. Both D/A fibers and the D control sample showed only a slight increase in temperature upon continuous illumination at 532 nm (Figure 5a). When the samples were irradiated at 808 nm, which corresponds to the $P3HT^{\bullet+}/F4TCNQ^{\bullet-}$ absorption bands, a significant temperature increase was observed for D/A nanofibers (Figure 5b). The photothermal effect in D/A fibers was more pronounced for longer nanofibers prepared at high concentrations or long incubation times (Figures 5c and S21). Note that the absorbance of D/A fibers at 532 and 808 nm are similar to the absorbance values of 0.538 and 0.403, respectively (Figure 1b). Therefore, the greater heat generation at 808 nm compared to 532 nm (Figure S22) suggests that the excited-state relaxation dynamics plays an important role in the photothermal response. As an additional control experiment, P3HT-*b*-PEO nanofibers were formed by adding a nonsolvent,

https://doi.org/10.1021/acsmacrolett.2c00752
ACS Macro Lett. 2023, 12, 382−388

ACN (40% in toluene), to the toluene solution of P3HT-*b*-PEO (0.05 mg/mL, Figure S23). The P3HT-*b*-PEO nanofibers without the acceptor showed only a slight temperature change when illuminated with 532 or 808 nm lasers (Figure S24).

In summary, a new type of highly doped semiconductor nanofiber was fabricated through self-assembly of P3HT-*b*-PEO diblock copolymers with F4TCNQ. P3HT-*b*-PEO spontaneously associated with electron-deficient F4TCNQ through ground state ICT interactions into 1D nanofibers. The self-assembly occurred in a good solvent for both D and A, which confirmed that the nanofibers were formed purely through ICT interactions. The D/A nanofibers exhibited characteristic $P3HT^{\bullet+}/F4TCNQ^{\bullet-}$ bands in the NIR region and complete quenching of P3HT photoluminescence. Control experiments with P3HT homopolymers and another BCP, P3HT-*b*-PDMS, showed no significant interaction at low concentrations and irregular precipitate formation at high concentrations. The results indicate that the PEO block along with the BCP architecture plays an important role in formation of well-defined self-assembly structures of D/A nanofibers. The efficient CT self-assembly of P3HT-*b*-PEO was attributed to the polar environment provided by the PEO shell, which could effectively stabilize ICT species. While the D/A nanofibers were stable over months at ambient conditions, they were responsive to various external stimuli including heat, chemicals, and light. In particular, D/A fibers showed efficient photothermal properties in the NIR region, providing a new avenue for the fabrication of efficient NIR photothermal agents.

EXPERIMENTAL SECTION

Synthesis of P3HT-*b*-PEO and P3HT-*b*-PDMS. P3HT-*b*-PEO and P3HT-*b*-PDMS were synthesized by the copper(I)-catalyzed click reaction between ethynyl-terminated P3HT and azide-terminated PEO or PDMS according to a previously published procedure.[20] Detailed synthetic procedures are provided in the Supporting Information

CT Self-Assembly. Stock solutions of P3HT-*b*-PEO (1 mg/mL) and F4TCNQ (0.5 mg/mL) were prepared separately in toluene and filtered through a 200 nm syringe filter. In a typical CT assembly, 100 μL of P3HT-*b*-PEO (1.89×10^{-4} M) and 200 μL of F4TCNQ (1.8×10^{-3} M) were mixed in a glass vial and heated at 60 °C for 5 min. Then, the mixture was diluted with toluene to reach desired P3HT-*b*-PEO and F4TCNQ concentrations. The CT solution was further aged for 12 h at room temperature under dark condition.

Photothermal Measurements. The D/A nanofibers in toluene were placed into a 5 mL glass vial. The temperature was measured with an infrared thermal camera at an interval of 1 min while irradiating with a 532 or 808 nm laser at 2.55 or 1.77 W/cm^2, respectively, for 10 min.

ASSOCIATED CONTENT

Supporting Information

The Supporting Information is available free of charge at https://pubs.acs.org/doi/10.1021/acsmacrolett.2c00752.

Detailed synthetic procedure and characterization data of P3HT-*b*-PEO and P3HT-*b*-PDMS, photophysical and morphological characterizations of D/A fibers, photothermal data of P3HT-*b*-PEO fibers (PDF)

AUTHOR INFORMATION

Corresponding Author

So-Jung Park − *Department of Chemistry and Nanoscience, Ewha Womans University, Seodaemun-gu, Seoul 03760, Korea;* orcid.org/0000-0002-6364-3754; Email: sojungpark@ewha.ac.kr

Authors

Karnati Narasimha − *Department of Chemistry and Nanoscience, Ewha Womans University, Seodaemun-gu, Seoul 03760, Korea;* orcid.org/0000-0001-5926-6274

Shine K. Albert − *Department of Chemistry and Nanoscience, Ewha Womans University, Seodaemun-gu, Seoul 03760, Korea;* orcid.org/0000-0002-0876-7316

Jongwook Kim − *Department of Chemistry and Nanoscience, Ewha Womans University, Seodaemun-gu, Seoul 03760, Korea*

Hyojung Kang − *Department of Chemistry and Nanoscience, Ewha Womans University, Seodaemun-gu, Seoul 03760, Korea*

Sungsu Kang − *School of Chemical and Biological Engineering, Institute of Chemical Process, Seoul National University, Seoul 08826, Republic of Korea; Center for Nanoparticle Research, Institute for Basic Science (IBS), Seoul 08826, South Korea*

Jungwon Park − *School of Chemical and Biological Engineering, Institute of Chemical Process, Seoul National University, Seoul 08826, Republic of Korea; Center for Nanoparticle Research, Institute for Basic Science (IBS), Seoul 08826, South Korea;* orcid.org/0000-0003-2927-4331

JaeHong Park − *Department of Chemistry and Nanoscience, Ewha Womans University, Seodaemun-gu, Seoul 03760, Korea;* orcid.org/0000-0002-0509-3934

Complete contact information is available at: https://pubs.acs.org/10.1021/acsmacrolett.2c00752

Author Contributions

§K.N. and S.K.A. contributed equally to this work.

Notes

The authors declare no competing financial interest.

ACKNOWLEDGMENTS

Financial support was provided from a National Research Foundation (NRF) of Korea Grant funded by the Korean government (NRF-2018R1A2B3001049) and by the Science Research Center (SRC) funded by the NRF (NRF-2017R1A5A1015365).

REFERENCES

(1) Kiefer, D.; Kroon, R.; Hofmann, A. I.; Sun, H.; Liu, X.; Giovannitti, A.; Stegerer, D.; Cano, A.; Hynynen, J.; Yu, L.; Zhang, Y.; Nai, D.; Harrelson, T. F.; Sommer, M.; Moulé, A. J.; Kemerink, M.; Marder, S. R.; McCulloch, I.; Fahlman, M.; Fabiano, S.; Müller, C. Double doping of conjugated polymers with monomer molecular dopants. *Nat. Mater.* **2019**, *18* (2), 149−155.

(2) Xu, K.; Sun, H.; Ruoko, T.-P.; Wang, G.; Kroon, R.; Kolhe, N. B.; Puttisong, Y.; Liu, X.; Fazzi, D.; Shibata, K.; Yang, C.-Y.; Sun, N.; Persson, G.; Yankovich, A. B.; Olsson, E.; Yoshida, H.; Chen, W. M.; Fahlman, M.; Kemerink, M.; Jenekhe, S. A.; Müller, C.; Berggren, M.; Fabiano, S. Ground-state electron transfer in all-polymer donor-acceptor heterojunctions. *Nat. Mater.* **2020**, *19*, 738.

(3) Liu, J.; Qiu, L.; Alessandri, R.; Qiu, X.; Portale, G.; Dong, J.; Talsma, W.; Ye, G.; Sengrian, A. A.; Souza, P. C. T.; Loi, M. A.; Chiechi, R. C.; Marrink, S. J.; Hummelen, J. C.; Koster, L. J. A. Enhancing Molecular n-Type Doping of Donor-Acceptor Copolymers by Tailoring Side Chains. *Adv. Mater.* **2018**, *30* (7), 1704630.

(4) Jacobs, I. E.; Moulé, A. J. Controlling Molecular Doping in Organic Semiconductors. *Adv. Mater.* **2017**, *29* (42), 1703063.
(5) Park, M.; Kang, S.; Nam, C.; Narasimha, K.; Lee, W. B.; Park, S.-J. Magnetic Field-Induced Self-Assembly of Conjugated Block Copolymers and Nanoparticles at the Air-Water Interface. *ACS Appl. Mater. Interfaces* **2022**, *14* (6), 8266−8273.
(6) Gregory, S. A.; Hanus, R.; Atassi, A.; Rinehart, J. M.; Wooding, J. P.; Menon, A. K.; Losego, M. D.; Snyder, G. J.; Yee, S. K. Quantifying charge carrier localization in chemically doped semiconducting polymers. *Nat. Mater.* **2021**, *20* (10), 1414−1421.
(7) Kim, M.; Ryu, S. U.; Park, S. A.; Choi, K.; Kim, T.; Chung, D.; Park, T. Donor-Acceptor-Conjugated Polymer for High-Performance Organic Field-Effect Transistors: A Progress Report. *Adv. Funct. Mater.* **2020**, *30* (20), 1904545.
(8) Jailaubekov, A. E.; Willard, A. P.; Tritsch, J. R.; Chan, W.-L.; Sai, N.; Gearba, R.; Kaake, L. G.; Williams, K. J.; Leung, K.; Rossky, P. J.; Zhu, X. Y. Hot charge-transfer excitons set the time limit for charge separation at donor/acceptor interfaces in organic photovoltaics. *Nat. Mater.* **2013**, *12* (1), 66−73.
(9) Tayi, A. S.; Shveyd, A. K.; Sue, A. C. H.; Szarko, J. M.; Rolczynski, B. S.; Cao, D.; Kennedy, T. J.; Sarjeant, A. A.; Stern, C. L.; Paxton, W. F.; Wu, W.; Dey, S. K.; Fahrenbach, A. C.; Guest, J. R.; Mohseni, H.; Chen, L. X.; Wang, K. L.; Stoddart, J. F.; Stupp, S. I. Room-temperature ferroelectricity in supramolecular networks of charge-transfer complexes. *Nature* **2012**, *488* (7412), 485−489.
(10) Pandeeswar, M.; Senanayak, S. P.; Narayan, K. S.; Govindaraju, T. Multi-Stimuli-Responsive Charge-Transfer Hydrogel for Room-Temperature Organic Ferroelectric Thin-Film Devices. *J. Am. Chem. Soc.* **2016**, *138* (26), 8259−8268.
(11) Kroon, R.; Mengistie, D. A.; Kiefer, D.; Hynynen, J.; Ryan, J. D.; Yu, L.; Müller, C. Thermoelectric plastics: from design to synthesis, processing and structure-property relationships. *Chem.Soc.-Rev.* **2016**, *45* (22), 6147−6164.
(12) Goel, M.; Thelakkat, M. Polymer Thermoelectrics: Opportunities and Challenges. *Macromolecules* **2020**, *53* (10), 3632−3642.
(13) Lim, E.; Peterson, K. A.; Su, G. M.; Chabinyc, M. L. Thermoelectric Properties of Poly(3-hexylthiophene) (P3HT) Doped with 2,3,5,6-Tetrafluoro-7,7,8,8-tetracyanoquinodimethane (F4TCNQ) by Vapor-Phase Infiltration. *Chem. Mater.* **2018**, *30* (3), 998−1010.
(14) Kroon, R.; Kiefer, D.; Stegerer, D.; Yu, L.; Sommer, M.; Müller, C. Polar Side Chains Enhance Processability, Electrical Conductivity, and Thermal Stability of a Molecularly p-Doped Polythiophene. *Adv. Mater.* **2017**, *29* (24), 1700930.
(15) Kiefer, D.; Yu, L.; Fransson, E.; Gómez, A.; Primetzhofer, D.; Amassian, A.; Campoy-Quiles, M.; Müller, C. A Solution-Doped Polymer Semiconductor:Insulator Blend for Thermoelectrics. *Adv.Sci.* **2017**, *4* (1), 1600203.
(16) Jacobs, I. E.; Bedolla-Valdez, Z. I.; Rotondo, B. T.; Bilsky, D. J.; Lewis, R.; Ayala Oviedo, A. N.; Gonel, G.; Armitage, J.; Li, J.; Moulé, A. J. Super-Resolution Photothermal Patterning in Conductive Polymers Enabled by Thermally Activated Solubility. *ACS Nano* **2021**, *15* (4), 7006−7020.
(17) Jacobs, I. E.; Aasen, E. W.; Nowak, D.; Li, J.; Morrison, W.; Roehling, J. D.; Augustine, M. P.; Moulé, A. J. Direct-Write Optical Patterning of P3HT Films Beyond the Diffraction Limit. *Adv. Mater.* **2017**, *29* (2), 1603221.
(18) Gao, J.; Niles, E. T.; Grey, J. K. Aggregates Promote Efficient Charge Transfer Doping of Poly(3-hexylthiophene). *J. Phys. Chem. Lett.* **2013**, *4* (17), 2953−2957.
(19) Méndez, H.; Heimel, G.; Winkler, S.; Frisch, J.; Opitz, A.; Sauer, K.; Wegner, B.; Oehzelt, M.; Röthel, C.; Duhm, S.; Többens, D.; Koch, N.; Salzmann, I. Charge-transfer crystallites as molecular electrical dopants. *Nat.Commun.* **2015**, *6* (1), 8560.
(20) Müller, L.; Nanova, D.; Glaser, T.; Beck, S.; Pucci, A.; Kast, A. K.; Schröder, R. R.; Mankel, E.; Pingel, P.; Neher, D.; Kowalsky, W.; Lovrincic, R. Charge-Transfer-Solvent Interaction Predefines Doping Efficiency in p-Doped P3HT Films. *Chem. Mater.* **2016**, *28* (12), 4432−4439.
(21) Kamps, A. C.; Fryd, M.; Park, S.-J. Hierarchical Self-Assembly of Amphiphilic Semiconducting Polymers into Isolated, Bundled, and Branched Nanofibers. *ACS Nano* **2012**, *6* (3), 2844−2852.
(22) Oh, S.; Yang, M.; Kang, S.; Chung, S.-H.; Bouffard, J.; Hong, S.; Park, S.-J. Binary Self-Assembly of Conjugated Block Copolymers and Quantum Dots at the Air-Liquid Interface into Ordered Functional Nanoarrays. *ACS Appl. Mater. Interfaces* **2019**, *11* (31), 28538−28545.
(23) Cativo, M. H. M.; Kim, D. K.; Riggleman, R. A.; Yager, K. G.; Nonnenmann, S. S.; Chao, H.; Bonnell, D. A.; Black, C. T.; Kagan, C. R.; Park, S.-J. Air-Liquid Interfacial Self-Assembly of Conjugated Block Copolymers into Ordered Nanowire Arrays. *ACS Nano* **2014**, *8* (12), 12755−12762.
(24) Shin, S.; Menk, F.; Kim, Y.; Lim, J.; Char, K.; Zentel, R.; Choi, T.-L. Living Light-Induced Crystallization-Driven Self-Assembly for Rapid Preparation of Semiconducting Nanofibers. *J. Am. Chem. Soc.* **2018**, *140* (19), 6088−6094.
(25) Foster, J. C.; Varlas, S.; Couturaud, B.; Coe, Z.; O'Reilly, R. K. Getting into Shape: Reflections on a New Generation of Cylindrical Nanostructures' Self-Assembly Using Polymer Building Blocks. *J. Am. Chem. Soc.* **2019**, *141* (7), 2742−2753.
(26) MacFarlane, L.; Zhao, C.; Cai, J.; Qiu, H.; Manners, I. Emerging applications for living crystallization-driven self-assembly. *Chem. Sci.* **2021**, *12* (13), 4661−4682.
(27) Gao, J.; Stein, B. W.; Thomas, A. K.; Garcia, J. A.; Yang, J.; Kirk, M. L.; Grey, J. K. Enhanced Charge Transfer Doping Efficiency in J-Aggregate Poly(3-hexylthiophene) Nanofibers. *J.Phys.chem.C* **2015**, *119* (28), 16396−16402.
(28) Reichstein, P. M.; Gödrich, S.; Papastavrou, G.; Thelakkat, M. Influence of Composition of Amphiphilic Double-Crystalline P3HT-b-PEG Block Copolymers on Structure Formation in Aqueous Solution. *Macromolecules* **2016**, *49* (15), 5484−5493.
(29) Jin, X.-H.; Price, M. B.; Finnegan, J. R.; Boott, C. E.; Richter, J. M.; Rao, A.; Menke, S. M.; Friend, R. H.; Whittell, G. R.; Manners, I. Long-range exciton transport in conjugated polymer nanofibers prepared by seeded growth. *Science* **2018**, *360* (6391), 897−900.
(30) Shaikh, H.; Jin, X.-H.; Harniman, R. L.; Richardson, R. M.; Whittell, G. R.; Manners, I. Solid-State Donor-Acceptor Coaxial Heterojunction Nanowires via Living Crystallization-Driven Self-Assembly. *J. Am. Chem. Soc.* **2020**, *142* (31), 13469−13480.
(31) Hicks, G. E. J.; Jarrett-Wilkins, C. N.; Panchuk, J. R.; Manion, J. G.; Seferos, D. S. Oxidation promoted self-assembly of π-conjugated polymers. *Chem.Sci.* **2020**, *11* (25), 6383−6392.
(32) Hicks, G. E. J.; Cranston, R. R.; Lotocki, V.; Manion, J. G.; Lessard, B. H.; Seferos, D. S. Dopant-Stabilized Assembly of Poly(3-hexylthiophene). *J. Am. Chem. Soc.* **2022**, *144* (36), 16456−16470.
(33) Jeffries-El, M.; Sauvé, G.; McCullough, R. D. Facile Synthesis of End-Functionalized Regioregular Poly(3-alkylthiophene)s via Modified Grignard Metathesis Reaction. *Macromolecules* **2005**, *38* (25), 10346−10352.
(34) Yim, K.-H.; Whiting, G. L.; Murphy, C. E.; Halls, J. J. M.; Burroughes, J. H.; Friend, R. H.; Kim, J.-S. Controlling Electrical Properties of Conjugated Polymers via a Solution-Based p-Type Doping. *Adv. Mater.* **2008**, *20* (17), 3319−3324.
(35) Huber, R. C.; Ferreira, A. S.; Thompson, R.; Kilbride, D.; Knutson, N. S.; Devi, L. S.; Toso, D. B.; Challa, J. R.; Zhou, Z. H.; Rubin, Y.; Schwartz, B. J.; Tolbert, S. H. Long-lived photoinduced polaron formation in conjugated polyelectrolyte-fullerene assemblies. *Science* **2015**, *348* (6241), 1340−1343.
(36) Narasimha, K. Macromolecular Effect Stabilized Color-Tunable and Room Temperature Charge-Transfer Complexes Based on Donor-Acceptor Assemblies. *ACS Appl. Polym. Mater.* **2020**, *2* (3), 1145−1159.
(37) Pingel, P.; Neher, D. Comprehensive picture of p-type doping of P3HT with the molecular acceptor F4TCNQ. *Phys. Rev. B* **2013**, *87* (11), 115209.
(38) Arvind, M.; Tait, C. E.; Guerrini, M.; Krumland, J.; Valencia, A. M.; Cocchi, C.; Mansour, A. E.; Koch, N.; Barlow, S.; Marder, S. R.; Behrends, J.; Neher, D. Quantitative Analysis of Doping-Induced

https://doi.org/10.1021/acsmacrolett.2c00752
ACS Macro Lett. 2023, 12, 382−388

Polarons and Charge-Transfer Complexes of Poly(3-hexylthiophene) in Solution. *J. Phys. Chem. B* **2020**, *124* (35), 7694−7708.
(39) Ghosh, R.; Chew, A. R.; Onorato, J.; Pakhnyuk, V.; Luscombe, C. K.; Salleo, A.; Spano, F. C. Spectral Signatures and Spatial Coherence of Bound and Unbound Polarons in P3HT Films: Theory Versus Experiment. *J.Phys.chem.C* **2018**, *122* (31), 18048−18060.
(40) Ghosh, R.; Luscombe, C. K.; Hambsch, M.; Mannsfeld, S. C. B.; Salleo, A.; Spano, F. C. Anisotropic Polaron Delocalization in Conjugated Homopolymers and Donor-Acceptor Copolymers. *Chem. Mater.* **2019**, *31* (17), 7033−7045.
(41) Enengl, C.; Enengl, S.; Pluczyk, S.; Havlicek, M.; Lapkowski, M.; Neugebauer, H.; Ehrenfreund, E. Doping-Induced Absorption Bands in P3HT: Polarons and Bipolarons. *ChemPhysChem* **2016**, *17* (23), 3836−3844.
(42) Samitsu, S.; Shimomura, T.; Heike, S.; Hashizume, T.; Ito, K. Effective Production of Poly(3-alkylthiophene) Nanofibers by means of Whisker Method using Anisole Solvent: Structural, Optical, and Electrical Properties. *Macromolecules* **2008**, *41* (21), 8000−8010.
(43) Tang, K.; McFarland, F. M.; Travis, S.; Lim, J.; Azoulay, J. D.; Guo, S. Aggregation of P3HT as a preferred pathway for its chemical doping with F4-TCNQ. *Chem.Commun.* **2018**, *54* (84), 11925−11928.
(44) Adhikari, S.; Spaeth, P.; Kar, A.; Baaske, M. D.; Khatua, S.; Orrit, M. Photothermal Microscopy: Imaging the Optical Absorption of Single Nanoparticles and Single Molecules. *ACS Nano* **2020**, *14* (12), 16414−16445.
(45) Wang, Y.; Zhu, W.; Du, W.; Liu, X.; Zhang, X.; Dong, H.; Hu, W. Cocrystals Strategy towards Materials for Near-Infrared Photothermal Conversion and Imaging. *Angew. Chem., Int. Ed. Engl.* **2018**, *57* (15), 3963−3967.
(46) Bisoyi, H. K.; Urbas, A. M.; Li, Q. Soft Materials Driven by Photothermal Effect and Their Applications. *Adv.Opt.Mater.* **2018**, *6* (15), 1800458.
(47) Cao, Y.; Dou, J.-H.; Zhao, N.-j.; Zhang, S.; Zheng, Y.-Q.; Zhang, J.-P.; Wang, J.-Y.; Pei, J.; Wang, Y. Highly Efficient NIR-II Photothermal Conversion Based on an Organic Conjugated Polymer. *Chem. Mater.* **2017**, *29* (2), 718−725.

https://doi.org/10.1021/acsmacrolett.2c00752
ACS Macro Lett. 2023, 12, 382−388